The Journal of Chemical Physics

Anisotropic diffusion of membrane proteins at experimental timescales

Cite as: J. Chem. Phys. **155**, 015102 (2021); https://doi.org/10.1063/5.0054973
Submitted: 23 April 2021 • Accepted: 17 June 2021 • Published Online: 02 July 2021

Matti Javanainen, Hector Martinez-Seara, Christopher V. Kelly, et al.

The Journal of Chemical Physics ARTICLE scitation.org/journal/jcp

Anisotropic diffusion of membrane proteins at experimental timescales

Cite as: J. Chem. Phys. 155, 015102 (2021); doi: 10.1063/5.0054973
Submitted: 23 April 2021 • Accepted: 17 June 2021 •
Published Online: 2 July 2021

Matti Javanainen,[1] Hector Martinez-Seara,[1] Christopher V. Kelly,[2] Pavel Jungwirth,[1] and Balázs Fábián[1,a)]

AFFILIATIONS

[1] Institute of Organic Chemistry and Biochemistry, Czech Academy of Sciences, Flemingovo nám. 542/2, 160 00 Prague 6, Czech Republic

[2] Department of Physics and Astronomy, Wayne State University, 666 W Hancock Street, Detroit, Michigan 48201, USA

[a)] **Author to whom correspondence should be addressed:** fbalazsf@gmail.com

ABSTRACT

Single-particle tracking (SPT) experiments of lipids and membrane proteins provide a wealth of information about the properties of biomembranes. Careful analysis of SPT trajectories can reveal deviations from ideal Brownian behavior. Among others, this includes confinement effects and anomalous diffusion, which are manifestations of both the nanoscale structure of the underlying membrane and the structure of the diffuser. With the rapid increase in temporal and spatial resolution of experimental methods, a new aspect of the motion of the particle, namely, anisotropic diffusion, might become relevant. This aspect that so far received only little attention is the anisotropy of the diffusive motion and may soon provide an additional proxy to the structure and topology of biomembranes. Unfortunately, the theoretical framework for detecting and interpreting anisotropy effects is currently scattered and incomplete. Here, we provide a computational method to evaluate the degree of anisotropy directly from molecular dynamics simulations and also point out a way to compare the obtained results with those available from SPT experiments. In order to probe the effects of anisotropic diffusion, we performed coarse-grained molecular dynamics simulations of peripheral and integral membrane proteins in flat and curved bilayers. In agreement with the theoretical basis, our computational results indicate that anisotropy can persist up to the rotational relaxation time $[\tau = (2D_r)^{-1}]$, after which isotropic diffusion is observed. Moreover, the underlying topology of the membrane bilayer can couple with the geometry of the particle, thus extending the spatiotemporal domain over which this type of motion can be detected.

I. INTRODUCTION

Proteins, either integral or peripheral, are potentially optimized for certain suitable environments to perform their functions. For example, protein oligomerization[1] and lipid–protein interactions—either via allosteric modulation[2] or membrane-mediation[3–6]—are central regulators of protein function. The formation of functional protein–protein and protein–lipid units is effectively driven by lateral diffusion along the membrane plane. Therefore, lateral diffusion coefficients of lipids and proteins are commonly extracted and used to characterize diffusion-limited processes in membranes.[7–9]

Protein and lipid diffusion measurements are increasingly used to uncover countless details on the molecular-level organization of cellular membranes. When combined with a proper theoretical framework, even indirect measurements reveal the presence of domains, compartmentalization, specific interaction patterns, and interleaflet coupling in the underlying membrane.[10–14] They manifest themselves as trapping, hopping, or anomalous diffusion modes.[15–17] All these phenomena have associated characteristic spatiotemporal scales and, therefore, certain experimental requirements for detection. Recent advances in super-resolution approaches[18] enabled diffusion measurements that reach nanometer spatial scales with a time resolution in the microsecond regime[13,19,20]—some even without the need to use any probes that could perturb the studied system.[21–23] Among these measurements, single-particle tracking (SPT) and high-speed AFM imaging[20,24,25] have been proven to be the most powerful approaches, as they provide a time series of molecular positions and/or orientations, which can be then analyzed using different theoretical models.

An aspect that has received little attention is the anisotropy of diffusive motion.[26,27] Anisotropy can stem from either an

anisotropic shape of proteins and protein complexes (hydrodynamic anisotropy) or the anisotropic interactions of proteins with the lipid bilayer (steric anisotropy).[28,29] The theoretical framework for particle anisotropy was already considered in the earliest works on diffusion, in the context of dielectric dispersion of ellipsoidal particles.[27,30] Since then, anisotropic diffusion has been addressed only by a fairly limited number of experimental and computational studies covering three-dimensional liquids.[26,31–37]

Based on hydrodynamic considerations, anisotropy of the diffusive motion in 2D is expected to be significantly larger than in 3D,[38] thus producing a more biologically relevant impact. This is intuitively explained by the fact that a 2D viscous medium must undergo large displacements in order to flow around the long, major axis of a particle. Contrary to this, 3D medium flow can always circumnavigate an elongated particle using the shorter particle dimensions, thereby reducing the hydrodynamic drag. Therefore, quasi-2D diffusion anisotropy of biomolecules is closer to the grasp of super-resolution techniques.[18] Moreover, cellular environments, such as macromolecular crowding, membrane domains, curvature, and confinement, should enlarge the affected spatiotemporal scales due to potentially delaying the onset of normal Brownian diffusion.[14–17,39–41] The Saffman–Delbrück (SD) model,[42] which provides a theoretical description of the lateral diffusion of membrane proteins, is the first place to look for hints and factors potentially favoring anisotropic diffusion in biological membranes. According to the SD model, the translational diffusion D_T is

$$D_T = k_B T b_T = k_B T \cdot \frac{1}{4\pi\eta_m h} \cdot \left(\ln \frac{\eta_m h}{\eta_s a} - \gamma \right), \tag{1}$$

where b_T is the translational mobility of the membrane inclusion, the η_s are the viscosities of solvent and the membrane, a is the radius of the diffusing particle, h is the thickness of the membrane, and γ is the Euler–Mascheroni constant (≈ 0.577). The rotational diffusion D_R is given by a similar expression

$$D_R = k_B T b_R = k_B T \cdot \frac{1}{4\pi\eta_m h} \cdot \frac{1}{a^2}. \tag{2}$$

These single diffusion coefficients, D_T and D_R, describe the ideal isotropic diffusion process that is time independent, or simply, they describe the long time limit behavior of the motion.

Rethinking the SD model in terms of a full diffusion tensor **D** instead of a single scalar diffusion coefficient reveals potential factors influencing anisotropy such as anisotropic membrane viscosity or asymmetric hydrophobic mismatch around the protein.[28] The non-circular shape of the membrane inclusion also influences diffusion, whether the diffuser is a single protein, a multimer, or a larger macromolecular complex. The extension of the SD model to anisotropic diffusion is not trivial. For example, diffusion parallel to the larger dimension of the particle is typically the least slowed down by hydrodynamic drag, indicating that it is the cross section of the particle in the plane perpendicular to a given axis that determines the magnitude of hydrodynamic interactions along the axis. On the other hand, treatment of the rotational diffusion of anisotropic particles does not require fundamental conceptual changes; it suffices to swap the square of the radius of the particle a^2 in the denominator by its anisotropic counterpart $a_1 \cdot a_2$ and introduce a "shape factor" to correct for the perturbed hydrodynamics.[43]

The anisotropic curvature in lipid bilayers[44] can create or enhance anisotropic diffusion by coupling with the asymmetry of the particle.[45] Cellular membranes experience varying mean and Gaussian curvatures on the <100 nm scale for the endoplasmic reticulum, mitochondria, vesicles, and on the plasma membrane during endocytosis/exocytosis.[46] The nanoscopic geometry of the membrane is frequently omitted in experiments and assumed to be flat. Curvature can manifest itself as an apparent anomalous and anisotropic diffusion in the laboratory frame,[39,40] potentially amplifying the effects of the anisotropic particle shape.

Single-particle tracking provides a molecular trajectory either directly or by following an attached probe.[22–24,47] Current experimental methods rarely provide information about the orientation of the diffusing particle. Notable exceptions are systems with multiple simultaneously tracked labels[48] or fluorescent methods that follow the orientation of the transition dipole moment.[49,50] Analysis of single-molecule location and orientation trajectories requires a theoretical foundation to connect studies of varying scales.

Molecular dynamics (MD) simulations can predict both the timescales and length scales of non-Brownian molecular motion and benchmark available theoretical frameworks with atomistic resolution.[51–53] Unlike other methods, such as Brownian dynamics simulations, that require as *a priori* input the anisotropic diffusion tensor to probe anisotropy,[29] MD simulations rely simply on the molecular interactions as parameters; thus, any resulting anisotropy is an inherent property of the studied system.

In this article, we perform MD simulations to show that inherent anisotropic diffusion arises from diffusing membrane-bound biomolecules of various shapes and that this effect can be magnified by the curvature of the membrane. We demonstrate this phenomenon and provide a theoretical method for SPT analysis. Our analysis allows automatic determination of the major and minor axes of a diffusing membrane-bound particle, given both position and orientation information vs time. It also provides a straightforward comparison of MD simulations with SPT experiments. Most notably, the anisotropic diffusion in our simulations extends into the spatiotemporal regime, which is within reach of modern super-resolution measurements and has possible biological significance. Our simulations do not give a detailed curvature dependence of the diffusion coefficient; however, the method could be applied to computational or experimental data to achieve that. Furthermore, our approach enables the experimental detection of structural information on the diffusing molecule (e.g., protein aggregation) and the host membrane (e.g., membrane curvature) through the analysis of diffusion anisotropy.

This article is organized as follows: First, we discuss the theory underlying the motion of anisotropic particles and introduce the "Fixed Initial Angle Mean Square Displacement" for determining the diffusion tensor. This is followed by the presentation of the fast converging *three-step relation* of Matsuda *et al.*,[54] which is considered to be a robust method to determine anisotropy from single particle experiments. The two methods are then applied to a range of systems: (a) passive rigid rotors of various sizes in a 2D argon liquid and (b) coarse-grained Martini models[55,56] of a peripheral F-BAR domain protein[57] and a transmembrane β-1 adrenergic receptor in its monomeric and dimeric forms,[58] each bound either to a planar or a curved lipid bilayer.

II. THEORY

A. Dynamics of an anisotropic particle

To derive the equations of motion for an anisotropic particle, one can consider the overdamped case of the Langevin equation

$$\dot{x} = \sqrt{2D} \cdot \xi(t), \tag{3}$$

where D is the isotropic translational diffusion coefficient and $\xi(t)$ is an independent correlation-free Gaussian random noise. This overdamped limit of the Langevin equation is the relevant regime to describe motion in viscous media, such as biomembranes, and it is, therefore, well suited for the analyses of molecular dynamics and SPT experiments on such systems.[59]

In the case of anisotropic lateral diffusion, one assigns different translational diffusion coefficients along the major ($D_\parallel$) and minor ($D_\perp$) axes of the diffusing particle, reflecting the different hydrodynamic radii. Such differences in radii are readily accessible, as demonstrated by several experimental and theoretical examples using particles with high aspect ratios.[34,60–62] The resulting Langevin equation for the motion of the particle—as derived by Han *et al.*[26]—can be found in Appendix A. One can also define the characteristic length (l), time (τ), and anisotropy of the motion (λ) as[60]

$$l = \left(\frac{D_\parallel + D_\perp}{2D_r}\right)^{1/2}, \ \tau = (2D_r)^{-1}, \ \lambda = \frac{(D_\parallel - D_\perp)}{(D_\parallel + D_\perp)}. \tag{4}$$

Following this set of equations, a particle tends to diffuse preferentially along a given direction on the timescale of τ until the translational correlation is washed out by rotation. Consequently, in planar systems, rotational averaging recovers the isotropic diffusion in the long time limit[26] with coefficient $D_{\text{long}} = (D_\parallel + D_\perp)/2$, respecting the isotropic nature of the membrane environment.

B. Detection of anisotropy in simulations

Consider the diffusion of an anisotropic particle that has $D_\parallel$ aligned with the x axis of the laboratory frame ($\phi_0 = 0$); ϕ_0 is the angle at which the particle diffuses fastest relative to the lab frame. The particle obviously shows larger individual displacements along the x axis than the y axis for lagtimes smaller than τ. Under these conditions, the initial diffusion coefficients measured along both axes will give $\lim_{\Delta\to 0} D_x(\Delta) = D_\parallel$ and $\lim_{\Delta\to 0} D_y(\Delta) = D_\perp$.

After some lagtime on the order of $\Delta \approx \tau$, the directional information is gradually lost due to rotational averaging. Eventually, in the long time limit $\Delta \gg \tau$, as a result of the central limit theorem, $D_x(\Delta) = D_y(\Delta) = (D_\parallel + D_\perp)/2$ is recovered, and isotropic diffusion is observed. This means that the information about the initial orientation of the particle, ϕ_0, can, in principle, be obtained on the timescale $\Delta \ll \tau$, albeit with less and less certainty as one approaches the timescale τ. Finally, by performing this tracking experiment several times, one can take an ensemble average over its many realizations. However, when an ordinary ensemble average is used, it constitutes an average over all possible initial angles, that is, over all possible ϕ_0. As generally it is not the underlying space but the particle itself that is anisotropic, this procedure results in isotropic diffusion, where the anisotropy is averaged out by the rotations. In other words, while at a fixed value of ϕ_0 the distribution of the individual displacements is asymmetric, the superposition—and subsequent averaging—of particles with different ϕ_0 orientations results in a symmetric distribution. Thus, to observe anisotropy, one must make sure to restrict the ensemble average to a fixed initial orientation.

While this recipe does allow the determination of anisotropic diffusion, the above described alignment of the particle requires *a priori* knowledge of the major and minor axes of the diffusing object. In molecular dynamics, one could take an arbitrary orientation ϕ_0 as the reference frame, such as the first configuration along the simulated trajectory. This angle ϕ_0 is the value by which the arbitrarily chosen reference frame must be rotated to correspond with the principal frame, where $D_\parallel = D_{xx}$ and $D_\perp = D_{yy}$. Then, before starting a mean square displacement (MSD) calculation the usual way, an root-mean-square deviation (RMSD) alignment must be performed to fit the current initial configuration ($\Delta = 0$), while also conceptually rotating along with it its whole trajectory, thereby transforming the displacements of the particle along with the particle itself into the reference frame. Once this is accomplished, the Fixed Initial Angle Mean Square Displacement (FIA-MSD)[26] can be evaluated as

$$\text{MSD}_{ij}(\Delta;\phi_0) = \langle[\Delta x_i(\Delta)][\Delta x_j(\Delta)]\rangle_{\phi_0}, \tag{5}$$

where $\langle\cdots\rangle_{\phi_0}$ denotes an ensemble average constrained to the initial angle ϕ_0. The FIA-MSD is related to the diffusion tensor $\mathbf{D}(\Delta;\phi_0)$ as

$$\text{D}_{ij}(\Delta;\phi_0) = \text{MSD}_{ij}(\Delta;\phi_0)/2t. \tag{6}$$

In general, the arbitrarily chosen reference frame and the principal frame in which the diffusion tensor is diagonal do not coincide, and thus, one must resort to rotating the reference sequentially for every single lagtime until the two frames align.

Because the diffusion tensor is just a covariance matrix, here we propose to diagonalize it at every lagtime by a suitable rotation matrix $\mathbf{R}(\Delta;\phi_0)$,

$$\mathbf{R}(\Delta;\phi_0)\mathbf{D}(\Delta;\phi_0)\mathbf{R}^{\text{T}}(\Delta;\phi_0) = \text{diag}(D_\parallel, D_\perp). \tag{7}$$

Explicit diagonalization of $\mathbf{D}(\Delta;\phi_0)$ provides $\mathbf{R}(\Delta;\phi_0)$ as a matrix formed by the eigenvectors of the matrix $\mathbf{D}(\Delta;\phi_0)$, with $D_\parallel$ and $D_\perp$ being the corresponding eigenvalues. As a result of this procedure, the off-diagonal elements are eliminated while the diagonals are given by $D_{xx} = D_\parallel$ and $D_{yy} = D_\perp$. Note that in the absence of anomalous diffusion, $D_\parallel$ and $D_\perp$ are independent of the lagtime.

This method for the evaluation of the anisotropy of translational diffusion is similar to the recent study of Linke *et al.*, who considered the 3D rotational diffusion of an anisotropic particle and performed a least squares fit of the covariance matrix to the ideal expressions[63] that assumes normal rotational diffusion. As even our simplest systems do not seem to exhibit ideal diffusion, here we considered an alternative approach to quantifying the error in our calculations: A peculiar attribute of diagonalizing the diffusion tensor at every time step is the fact that the algorithm is guaranteed to find a "largest" and "smallest" axis in the dataset. In practice, this prevents $D_\parallel$ and $D_\perp$ from converging to the same value for isotropic particles, as the algorithm will find small numerical differences along certain axes in the data and assign the larger (smaller) value to $D_\parallel$ ($D_\perp$). By performing the eigenvalue calculation at a given value of lagtime Δ, one obtains an *estimate* of the angle ϕ_0, corresponding to the diagonalization of $\mathbf{D}(\Delta;\phi_0)$ at that lagtime. Of course, the real particle should only be characterized by a single real ϕ_0. Hence, while a mostly constant estimate of the angle ϕ_0 (as a function lagtimes up

to the timescale τ) signifies anisotropic motion, large changes indicate that only statistically insignificant differences in the diffusion tensor have been found by the diagonalization. The estimate of ϕ_0 becomes less accurate for particles with less anisotropy, for longer lagtimes, and for shorter simulations. Finally, the best estimate of ϕ_0 is calculated as an average on the range $\Delta \ll \tau$. After averaging, the $\langle\phi_0\rangle$ is subsequently used in Eq. (5) to once more decompose the diffusion tensor at various lagtimes and thus reanalyze the trajectory.

C. Detection of anisotropy from experiments

Several theoretical tools exist for the evaluation of particle anisotropy in SPT experiments.[54,60,61] To provide means for comparing the simulated results to experiments, we implemented the three-step relation of Matsuda *et al.*, which was proven to have smaller errors and faster rate of convergence than other existing approaches.[54]

In their algorithm, Matsuda *et al.* considered relative displacements between three consecutive positions. From the relative displacements, a scatter plot is calculated. The deviation from a circular distribution is then quantified by a radius of gyration tensor (denoted by $\langle R_r^2\rangle$), as discussed in Appendix C. Although the exact relationship between $\langle R_r^2\rangle$ and the degree of anisotropy λ is unknown, the authors provide a simple polynomial equation fitted to results simulated at different values of λ and $\Delta t'$, the non-dimensionalized time step.[54] Despite the quadratic relation describing the connection between $\langle R_r^2\rangle$ and λ, the equation [Eq. (17) in Ref. 54] is a one-to-one mapping, and therefore, it can be readily inverted to express λ in terms of $\langle R_r^2\rangle$. This inverse reads

$$\lambda(R_r^2, \Delta t) = -\frac{(p_{10} + p_{11}\Delta t)}{2p_{20}} + \sqrt{\frac{(p_{10} + p_{11}\Delta t)^2}{4p_{20}^2} - \frac{(1 - R_r^2)}{p_{20}}}, \quad (8)$$

with parameters

$$p_{10} = (-1.41 \pm 2.28) \times 10^{-2}, \quad (9)$$

$$p_{20} = -0.897 \pm 0.028, \quad (10)$$

and

$$p_{11} = -1.44 \pm 0.16 \quad (11)$$

taken from the original publication (Ref. 54). This expression provides a convenient relationship to compare anisotropy values obtained from computer simulations and SPT experiments. To distinguish between the two ways of calculation, we designated with λ_{MD} and λ_{SPT} the values calculated from molecular simulations and SPT analysis, respectively. It is important to point out that while both methods can provide information about the degree of anisotropy of the diffusing particle, only the molecular method gives direct access to the diffusion coefficients along the major and minor axes of the particle.

III. METHODS

A. Simulations

MD simulations of a 2D model Lennard-Jones (LJ) liquid with various inclusions and extensive coarse-grained (CG) Martini[55] simulations were performed with the GROMACS 2020 package[64,65] to evaluate the degree of diffusion anisotropy in molecular systems.

The LJ systems investigated here are similar to those used by Jeon *et al.*[66] The LJ beads were parameterized to represent argon atoms, with $\sigma = 0.3405$ nm and $\varepsilon = 0.996$ kJ/mol.[67] Simulations were performed in the canonical NVT ensemble (essentially NAT with a fixed area, A, as all particles were initially positioned on a plane and remained there) at the boiling temperature of argon (87.3 K), and the area of the simulation box was chosen to approximately reproduce the 3D diffusion coefficient of argon at 1 bar pressure. In order to investigate the effect of particle anisotropy in simple systems, we have simulated the following argon systems: (I) 2D argon without inclusions, (II) 2D argon with a four-bead linear rotor (connected by rigid bonds), (III) 2D argon with a six-bead linear rotor, (IV) 2D argon with an eight-bead linear rotor, and (V) 2D argon with a hexagonal inclusion of seven beads. The geometry of the linear rotors was held fixed by virtual sites, which prevented any "buckling" of the particles. It is important to note that the term "rotor" in this context does not imply any active mechanism. For each case, 1000 solvent molecules were used in 100 ns long simulations, performed with a 1 fs step size and repeated five times. The temperature of the systems was controlled by the stochastic velocity rescaling algorithm algorithm,[68] while the simulation box dimensions were $L_x = L_y = 11.6$ nm and $L_z = 4$ nm. No charges were present, and the LJ interactions were truncated at 1 nm, which ensured that all interactions took place along the 2D plane.

To investigate more realistic systems containing proteins, CG Martini[55,56] simulations of a peripheric F-BAR domain (PDB id: 2V0O)[69] and the B_1-adrenergic receptor (PDB id:4GPO)[58] monomer (B_1-AR-m chain B) and dimer (B_1-AR-d chains A & B) were performed in bilayers composed of POPC lipids (Fig. 1). These bilayers were fully hydrated, and 10% of the solvent was modeled as the antifreeze particles to prevent the well-known crystallization of the solvent in the Martini force field.[55] Ions were used to neutralize any excess charge of the proteins. Although F-BAR is not an integral membrane protein, it might still exhibit anisotropic lateral diffusion due to its association with the membrane and its highly asymmetric shape. F-BAR is known to interact strongly with negatively charged lipids.[70] However, as we have not found any clear difference between such membranes and neat PC, we chose to use the neat PC for all simulations in this work. The dimeric B_1-AR protein is a transmembrane complex that also has an asymmetric shape, while the monomeric form is essentially cylindrical and thus expected to diffuse isotropically. To quantify the impact of curvature on the diffusion coefficient observed in SPT experiments, we simulated the proteins in both planar and curved bilayers. The curved membranes were generated by the BUMPy script[71] and maintained by dummy particles that repelled the acyl chains. The 50 μs long simulations were performed using the *New-RF* Martini simulation parameters[72] with a time step of 25 fs. The input parameters are available under the DOIs listed in Table III. As a reference for the curved systems, a similar system was simulated without any additional proteins, for 20 μs. Overall, more than 600 μs of CG simulations were performed

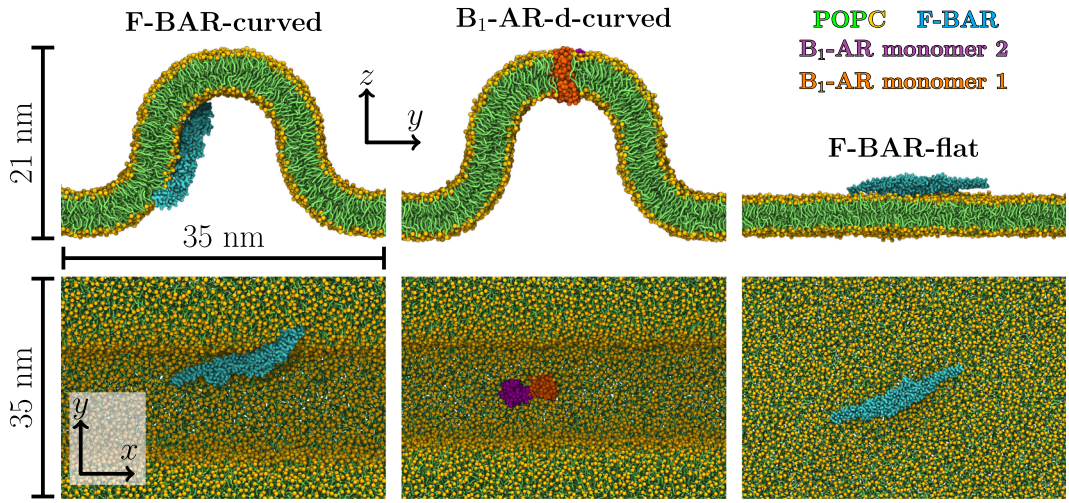

FIG. 1. Side (top row) and top (bottom row) views of the final conformations of three coarse-grained systems (see Table I for naming). Protein coloring in the legend. In POPC, the choline (NC3) bead is shown in yellow, whereas the rest of the molecule is shown in green. Water, counter-ions, and the dummy particles that are used to maintain the curved membrane conformation are not shown for clarity. The shown systems are chosen as examples: B_1AR-m-curved is identical to B_1AR-d-curved but with only one protein monomer. B_1AR-m-flat and B_1AR-m-flat are identical F-BAR-flat but with the protein monomer or dimer embedded in the bilayer instead of the F-BAR bound onto it. The size bars are for the curved membranes, yet the flat ones cover a very similar area of 37×37 nm^2.

in the framework of this study. A summary of all systems can be seen in Table I.

B. Anisotropic diffusion

For the computation of the FIA-MSD, the first frame of the first replica of every simulated trajectory of every inclusion-type was considered as a reference. This way, the same reference orientation was used to analyze all replicas of F-BAR/B_1-AR in both the curved and flat systems. Then, the rotation matrix required for the least-squares fitting of the given conformation onto the reference was computed. As the observable of interest is inherently two dimensional, the rotation matrix was calculated over the system projected onto the macroscopic plane of the membrane. While this is trivial in the case of B_1-AR, the possible rotation along the major axis (along the axis lying in the macroscopic plane of the bilayer) of F-BAR causes the rotation matrix to spuriously switch signs. To avoid this, the orientation of F-BAR was calculated based on two representative points of the protein backbone.

Using the orientation encoded in the rotation matrix, the FIA-MSD was evaluated by aligning the particle at lagtime $\Delta = 0$ with the reference while also rotating its trajectory along with it. This

TABLE I. Summary of the simulated 2D argon "toy model" and coarse-grained Martini systems.

Name	Inclusion	Solvent	Length	Replicas
		2D argon		
Rotor 4	4-bead	1000 Ar	500 ns	5
Rotor 6	6-bead	1000 Ar	500 ns	5
Rotor 8	8-bead	1000 Ar	500 ns	5
Disk	7-bead	1000 Ar	500 ns	5
		CG Martini		
F-BAR-flat	F-BAR	4000 POPC	50 μs	2
F-BAR-curved	F-BAR	6108 POPC	50 μs	2
B_1-AR-m-flat	B_1-AR monomer	4000 POPC	50 μs	2
B_1-AR-m-curved	B_1-AR monomer	6108 POPC	50 μs	2
B_1-AR-d-flat	B_1-AR dimer	4000 POPC	50 μs	2
B_1-AR-d-curved	B_1-AR dimer	6108 POPC	50 μs	2

way, the particle always started diffusion from the same initial orientation, albeit not the one corresponding to the principal frame, but an arbitrarily chosen one. Having calculated the FIA-MSD, the orientation of the principal frame (where the MSDs along the two axes are uncorrelated, thus the diffusion coefficients are decoupled) with respect to the reference frame was obtained by diagonalization of the reference-frame MSD tensor based on Eq. (7). This procedure provides not only the diagonal values $D_\parallel$ and $D_\perp$ at every lagtime but also an associated angle. Note that the diffusion coefficients presented in this work were not corrected for finite-size effects,[73] as we are interested in the general phenomenon of anisotropic diffusion and not the absolute magnitude of the coefficients. Furthermore, the diffusion coefficients reported for the curved systems were obtained by projecting the motion of the particles onto the macroscopic plane of the bilayer.

For the principal frame to be meaningful, this angle must be constant for lagtimes up to the characteristic time of anisotropic diffusion. Of course, finite statistics and the molecular flexibility of the particles add noise to ϕ_0. To eliminate this effect, we calculated the average $\langle\phi_0\rangle$ over an interval of lagtimes and across replicas and performed a second decomposition similar to Eq. (7) but using $\langle\phi_0\rangle$ without lagtime-dependence.

Furthermore, the three-step relation of Matsuda *et al.*[54] was also implemented along with the inverted relationship between $\langle R_r^2\rangle$ and λ. These two methods provide a convenient way to compare computationally and experimentally available data. The source code written in Python for these two procedures is freely available on GitHub at https://github.com/balazsfabian/MD_anisotropy.

IV. RESULTS AND DISCUSSION

A. A model system: 2D argon

As a simple model system, we have analyzed the behavior of solutes in a 2D argon liquid. Despite being only two dimensional and thus lacking any surrounding medium, such two-dimensional systems still qualitatively capture the Saffman–Delbrück scaling relations in terms of rotational and translational dynamics.[41,74] Moreover, their diffusion behavior has been demonstrated to agree with coarse-grained and atomistic models of lipid membranes.[51,66] However, following the Stokes' paradox, diffusion coefficients in a two-dimensional fluid diverge with increasing system sizes, as there is no solvent through which momentum could be transferred. This issue also haunts simulations of quasi-two-dimensional lipid bilayers with limited amounts of solvent. In that case, however, a theoretical framework exists for the extrapolation of diffusion coefficients to infinite system sizes in terms of lateral dimensions as well as the height of the solvent layer.[75] Still, the 2D argon liquid is a suitable simplification for a qualitative study of anisotropic diffusion, where absolute values of the diffusion coefficients are not central. In the case of passive linear rotors, the major and minor axes of anisotropic diffusion are immediately obvious from symmetry considerations. The diffusion coefficients according to Eq. (6) and the calculated orientation of the principal frame with respect to the reference frame—that is the angle between the major axis of the particle and the x axis of the simulation box—can be found for all the systems in Fig. 2. For the sake of simplicity, the reference and principal frames were made to coincide by choosing a reference where the major axis of the particle was aligned with the x axis of the simulation box. The largely constant value of ϕ_0 across replicas and up to lagtimes on the order of the characteristic time of anisotropic diffusion (τ) are indicative of anisotropic diffusion even for the smallest solutes. This clearly contrasts the case of the circular disk for which neither a single curve of a given replica nor the different replicas converge to a common orientation (see Fig. 2). The diffusion coefficients present a similar picture, namely, the diagonalized diffusion tensors are anisotropic, and the diffusion coefficients $D_\parallel$ and $D_\perp$ are centered symmetrically around the isotropic value D. Furthermore, they tend to converge to the average diffusion coefficient D

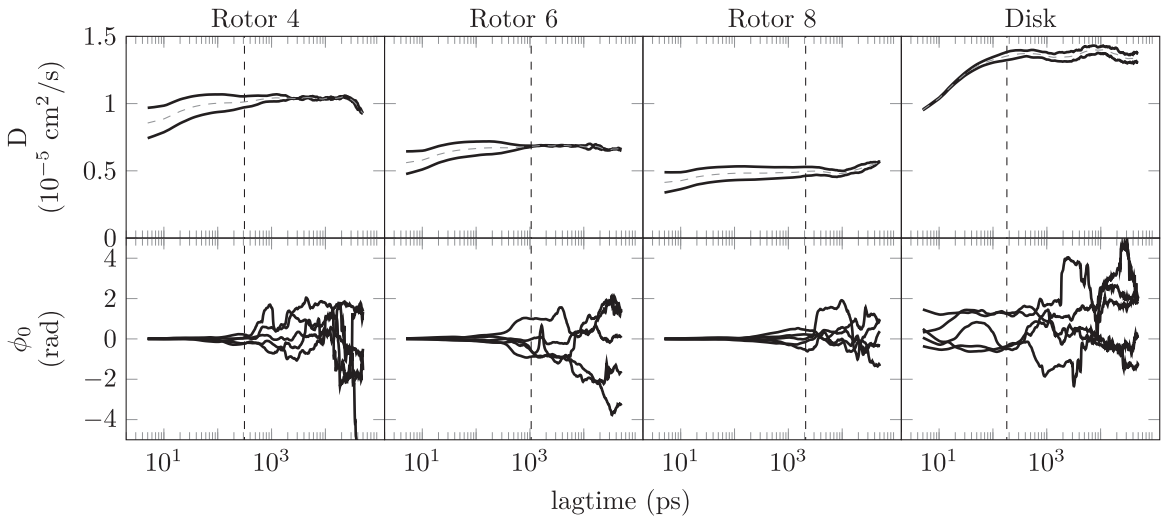

FIG. 2. (Top) Lateral diffusion coefficients of the various inclusions simulated in a 2D argon fluid. The solid black curves represent the diffusion coefficients along the major and minor axes of the particle ($D_\parallel$ above, $D_\perp$ below), while the dashed line is the isotropic value (D). (Bottom) Angle formed by the major axis of the particle between the principal and reference frames. The different curves correspond to the five replicas. The red dashed vertical line corresponds to the timescale of anisotropic diffusion (τ).

on the timescale τ before diverging because of the lack of statistics. The behavior of the circular disk is again qualitatively different, as $D_\parallel$ and $D_\perp$ initially coincide and gradually diverge as the statistics worsens.

The overall diffusion in the 2D LJ systems with/without solutes closely matches the behavior observed in Jeon *et al.*,[51] namely, an initial regime of superdiffusion apparent from the upward curving MSD (not shown here) followed by normal diffusion. In these simple 2D liquids, the surrounding medium is isotropic, so there should be no *direct* coupling between anomalous and anisotropic diffusion, although the presence of anomalous behavior clearly influences the observed degree of anisotropy by changing the isotropic diffusion coefficient. In addition to the anomalous isotropic diffusion coefficient, $D_\parallel$ and $D_\perp$ are distinctly different from the ideal case represented by Eq. (B1) (see Appendix B), even after the subtraction of the anomalous isotropic term D.

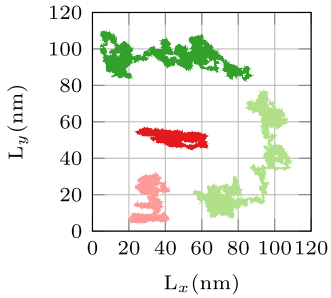

FIG. 3. Trajectories of the simulated CG F-BAR domains projected onto the macroscopic plane of the membrane. Green and light green represent the two replicas of the flat system, while those of the curved system are colored in red and pink. The repeat distance along the curved y axis is ≈34 nm. The trajectories are arbitrarily shifted for visualization.

B. A peripheral protein: F-BAR domain

To investigate the effects of anisotropy on the dynamics in a more biologically relevant setting, we first evaluated diffusion of the F-BAR domain attached onto flat and curved membranes. The trajectories of all the replicas projected onto the xy plane can be seen in Fig. 3. The area covered by the particle in the flat system is much larger than in the curved one. In addition, in the case of curved membranes, the geometric restriction imposed on the particle by the curvature of the bilayer is apparent from the horizontal "slabs" in the plot of the trajectory. Interestingly, the distance between these slabs does not correspond to the wavelength of the curved surface. It is merely an artifact of projecting the inherently 3D motion of the particles onto the macroscopic plane of the bilayer, albeit amplified by the anisotropic motion of the proteins and their curvature preference. More explicitly, the major axis of the particle tends to be parallel to the x axis of the laboratory resulting in large displacements along the x axis, while the displacements along the minor axis are further decreased as a result of the projection.

First, we computed the Mean Square Rotation (MSR) of F-BAR in all of the simulated system and extracted the rotational diffusion coefficients D_r from linear fits on the range between 100 ns and 1 μs. The obtained values are presented in Table II, while the log–log plot of the curves can be seen in the top panel of Fig. 4. On the surface of the flat membrane, the F-BAR can rotate freely and rapidly. However, on the curved bilayer, its rotation is highly constrained by the geometry of the membrane, as supported by a more than ten-fold decrease in the rotational diffusion coefficient and a subdiffusive anomalous diffusion exponent.[59] The characteristic timescales of anisotropy τ computed from D_r are shown in Table II. It must be noted that even though a τ value can be calculated for any particle, it represents the relevant timescale only for a particle that has an appreciable degree of anisotropy λ. According to these values, the anisotropy of the F-BAR domains can be detected on a 1 μs timescale in the planar case and on a 10 μs timescale in the curved one. Therefore, based on our simulations, its temporal scale puts anisotropy within reach of experimentally measurable quantities.[48,76,77]

To further characterize the rotational dynamics of the F-BAR, we calculated the probability density function of its 2D orientation in the macroscopic plane of the membranes. The angle was taken to be formed by the x axis of the laboratory frame of reference and the major axis of diffusion, the determination of which is discussed below. The calculated curves are presented in the top panel of Fig. 5. The results related to the planar bilayers reinforce the idea that the anisotropic motion of the particle does not in any measure induce anisotropy in the plane of the membrane. The situation is quite the opposite, as it is the curved lipid bilayer that exerts forces that

TABLE II. Major, minor, isotropic, and rotational diffusion coefficients and anisotropy parameters calculated "from MD" (λ_{MD}) and "from SPT"(λ_{SPT}) for the F-BAR and B_1-AR monomer and dimer proteins in flat and curved POPC bilayers. The translational diffusion coefficients were averaged from 10 to 100 ns, whereas D_r was averaged 100 ns to 1 μs. λ_{MD}, l, and τ are derived from the diffusion coefficient following Eq. (4), while λ_{SPT} is obtained by the three-step relation of Matsuda *et al.*[54]

	Translational diffusion (10^{-8} cm^2/s)							
Name	$D_\parallel$	$D_\perp$	D	D_r (10^5 rad^2/s)	λ_{MD}	λ_{SPT}	l (nm)	τ (μs)
F-BAR-flat	21.1 ± 0.9	14.2 ± 0.6	17.7 ± 0.6	5.2 ± 0.7	0.19 ± 0.04	0.26 ± 0.04	5.9 ± 0.4	1.0 ± 0.1
F-BAR-curved	10.9 ± 2.4	3.2 ± 0.1	7.0 ± 1.2	0.4 ± 0.1	0.54 ± 0.09	0.48 ± 0.02	13.9 ± 3.4	13.2 ± 4.2
B_1-AR-m-flat	18.0 ± 0.4	17.2 ± 0.7	17.6 ± 0.3	26.0 ± 0.3	0.02 ± 0.01	0.05 ± 0.04	2.6 ± 0.1	0.2 ± 0.1
B_1-AR-m-curved	8.4 ± 0.7	5.9 ± 0.2	7.1 ± 0.4	6.2 ± 1.3	0.17 ± 0.06	0.13 ± 0.04	3.4 ± 0.3	0.8 ± 0.2
B_1-AR-d-flat	13.8 ± 0.4	11.3 ± 0.1	12.6 ± 0.2	11.6 ± 0.8	0.09 ± 0.01	0.18 ± 0.05	3.3 ± 0.1	0.4 ± 0.1
B_1-AR-d-curved	6.5 ± 0.3	3.2 ± 0.2	4.9 ± 0.2	0.3 ± 0.1	0.35 ± 0.01	0.21 ± 0.02	18.0 ± 8.7	16.9 ± 0.1

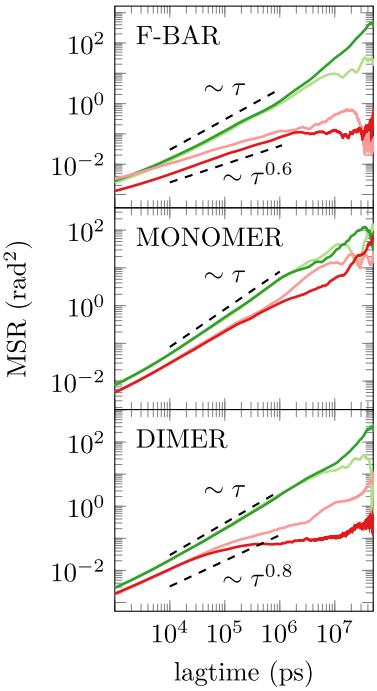

FIG. 4. Mean Square Rotation of the various inclusions in the flat (green and light green) and curved (red and pink) POPC bilayers. Dashed lines represent different values of the anomalous diffusion exponent[59] $\langle \phi^2(\Delta) \rangle = D_\alpha \Delta^\alpha$. Linear fits of D_r were made on the range from 100 nm to 1.0 μs.

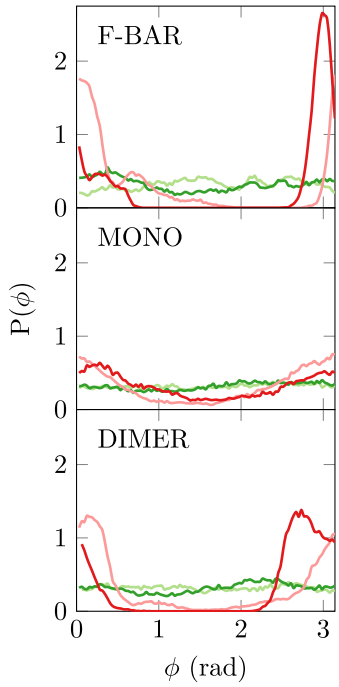

FIG. 5. Probability density function of the protein orientation in the flat (green and light green) and curved (red and pink) POPC bilayers. The angle ϕ is taken to be the angle between the major axis of diffusion and the x axis of the laboratory frame. In all cases, the proteins exhibit free rotation in the flat systems. This is in contrast to that observed in the curved systems, where the preferred orientation of the major axis of the particle coincides with the non-curved x axis.

restrain the free rotation of F-BAR, thereby increasing the degree of anisotropy in its motion.

The next step of the analysis was the calculation of the FIA-MSDs and diffusion tensors by Eqs. (5) and (6), as described in the Methods section. Upon diagonalization of the diffusion tensor at every lagtime, one finds that the angles between the principal and reference frames remain constant almost up to τ and agree closely with each other in the two replicas, as seen in the top panel of Fig. 6. The translational diffusion coefficients obtained through the diagonalization are presented in the top panel of Fig. 7 (red dashed lines). In order to emphasize the uniqueness of the major axis of the particle, the curves in Fig. 7 were recalculated using $\langle \phi_0 \rangle$ as averaged across both replicas from 10 to 100 ns (black lines). Considering that the obtained curves show an appreciable degree of anomalous diffusion, which also has an impact on the anisotropy [at least through the denominator of λ, see Eq. (4)], we also fitted the diffusion coefficients between 10 and 100 ns, which proved to be a suitable compromise to minimize the effects of anomalous behavior, while still being smaller than τ. The major, minor, and isotropic diffusion coefficients can be found in Table II.

The characteristic quantities of the anisotropic diffusion calculated from the diffusion coefficients are collected in Table II. Similar to the τ values, the characteristic lengthscale l of anisotropic diffusion also falls in the regime of experimental methods.[20,48,76,77] The orientational constraint imposed on F-BAR by the curved bilayer greatly reduces both the translational and rotational diffusion of the protein while increasing the timescales and length scales of the anisotropic behavior. In particular, the measured degree of anisotropy of the motion is enhanced by the decrease in the isotropic diffusion coefficient accompanied by similar differences between the diffusion along the major and minor axes of the protein.

For the sake of comparison, the degree of anisotropy measured by Han *et al.* for a prolate ellipsoid with an aspect ratio of 8:1 (radii $r_1 = 2.4\ \mu$m and $r_2 = r_3 = 0.3\ \mu$m[26]) was found to be $\lambda = 0.605$, which is commensurate with the value $\lambda_{MD} = 0.54$ obtained for the F-BAR whose ratio is ~5:1 (radii $r_1 = 18$ nm and $r_2 = r_3 = 3.3$ nm).

C. Transmembrane proteins: Monomer and dimer of the β_1-adrenergic receptor

To cover a wider range of scenarios, we also simulated the B_1-AR monomer and dimer in the flat and curved bilayers. Similar to the F-BAR domain, we calculated the mean squared rotation, as seen in Fig. 4. The B_1-AR dimer exhibits anomalous rotational diffusion in the curved system, possibly owing to the more constrained rotation compared to the monomer. Correspondingly, going from the planar to the curved membrane, the rotational diffusion coefficient decreases about four-fold for the monomer, but 30-fold for the dimer, which is an even larger change than in the case of F-BAR. This is also supported by the angle distribution (see Fig. 5), where only a mild angle preference can be observed for the monomer, but rather a strong one in the case of the B_1-AR dimer. The rotational diffusion coefficients can be found in Table II.

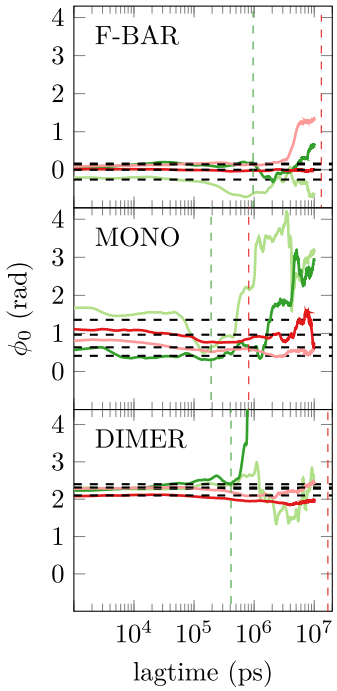

FIG. 6. The angle ϕ_0 representing the major axis of diffusion of the particle as a function of the lagtime τ in the flat (green and light green) and curved (red and pink) POPC bilayers. Vertical dashed lines: characteristic timescales of anisotropic diffusion as computed from the D_r values, with the green line corresponding to flat and the red line to the curved systems. Horizontal dashed lines: values of ϕ_0 averaged between 100 ns and 1.0 μs for the individual replicas. In all of the systems presented, the value of ϕ_0 remains fairly constant in lagtime and across replicas, with the exception of the B_1-AR monomer on the flat membrane. In the latter, there are significant differences in lagtime as well as between the individual replicas.

The FIA-MSDs were also computed in the same manner as for the F-BAR domain. The ϕ_0 values representing the angle between the instantaneous major axis and the x axis of the laboratory frame of reference agree closely among the replicas and for varying lagtimes, with the exception of the B_1-AR monomer in the flat membrane. The 2D projection of this protein is close to circular and, therefore, its motion is expected to be isotropic, as supported by our results.

The diffusion coefficients along the major and minor axes of the particle show clear anisotropy for the dimer in both geometries and present strong evidence for the isotropy of the monomer in the flat membrane. The curved system exhibits hints of anisotropic behavior; however, the diffusion coefficients at short lagtimes are fairly close to each other. Based on the argon "toy model" system, the proximity of these two curves at small lagtimes is a hallmark of isotropic behavior, as indicated by the circular disk data in Fig. 2. Therefore, the anisotropic diffusion of the B_1-AR monomer in the curved system cannot be definitively stated. The various translational diffusion coefficients are collected in Table II.

Just as for F-BAR, the curvature of the membrane increases the length scale and timescale and the degree of anisotropy for both the B_1-AR monomer and dimer. The values can be found in Table II. The differences seem to originate from the slower isotropic and rotational diffusion of the proteins, while maintaining the differences between the major and minor axes. Notably, the ratios of the diffusion coefficients of the dimers and the monomers are always $\approx 70\%$. In the framework of the Saffman–Delbrück model for cylindrical diffusers, this difference suggests that a dimer would have twice the hydrodynamic radius of a monomer [$D \sim \ln(R)$] according to Eq. (1).[42] This seems somewhat excessive, especially as the dimers and monomers are expected to have similar hydrodynamic radii along the parallel axis, which dominates the dimer diffusion ($D_\parallel > D_\perp$). Nevertheless, we are not aware of a general theoretical framework that would describe the lateral diffusion of non-cylindrical proteins.

D. Effect of curvature on anisotropic diffusion

When taking into account the orientational preference of the particle as seen in Fig. 5, one can consider the curved membrane as an external, position dependent torque on the peripheral F-BAR domain, reminiscent of the theoretical setups considered by Grima and Yaliraki.[78] However, the idealizations implicit in the derivation of their equations prevent meaningful comparison with the present results. For example, in our simulations just as in reality, the interactions between the proteins and the membrane differ in the two environments.

In order to investigate the effect of the curvature, we computed the lateral diffusion coefficients of the lipids along the x and y axes separately in the neat, curved system. The obtained values are $D_{x,\text{lipids}} = 6.35 \times 10^{-7}$ cm^2/s and $D_{y,\text{lipids}} = 2.43 \times 10^{-7}$ cm^2/s, with D_x being in accord with the literature value of isotropic diffusion for lipids on planar membranes, in the Martini model.[41] Remarkably, the isotropic D of the proteins is always decreased by curvature according to the geometric ratio[79] $D_{y,\text{lipids}}/D_{x,\text{lipids}} \approx 0.4$. Even though the anisotropic diffusion coefficients show no such clear tendencies, the degree of anisotropy is always enhanced by the curvature of the membrane or even induced, as observed for the B_1-AR monomer.

A peculiar feature of the rotationally constrained diffusion of the F-BAR domain is that $D_x > D_\parallel$ and $D_y < D_\perp$ (see Fig. 7). This finding seemingly contradicts the fact that during the anisotropic diffusion, $D_\parallel$ ($D_\perp$) should be maximal (minimal). The apparent contradiction stems from the anisotropy of the environment and can be resolved by the following picture: the rotationally constrained particle is predominantly oriented along the x axis, so its $D_\parallel$ value is unhindered compared to $D_\perp$, which lies against the crests of the membrane. Rotating away from this preferred orientation by a small angle points the major axis of the particle toward the crests of the undulating membranes, and thereby, the translation along the major axis decreases. Although in this arrangement, the diffusion also decreases along the x axis, but only to a lesser extent.

E. Comparison of experimental and simulation approaches

To provide more direct means for experimental comparison, we have implemented the three-step relation of Matsuda *et al.*,[54] which requires as input only the rotational diffusion coefficient and the particle trajectory as measured in SPT. Matsuda *et al.* detected diffusion anisotropy with a weak dependence on the value of D_r such

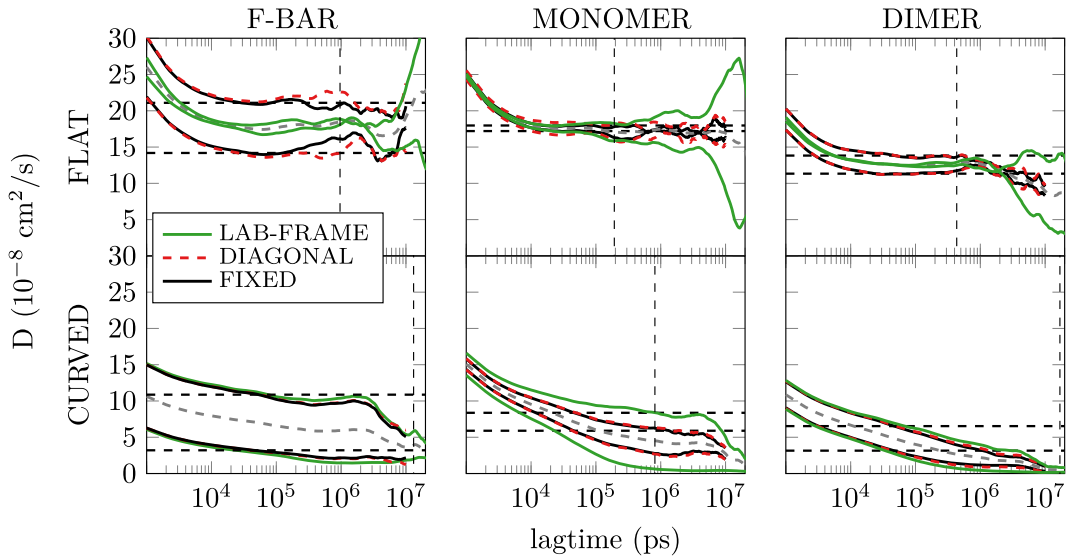

FIG. 7. Lateral diffusion coefficients of the F-BAR, B_1-AR monomer, and dimer proteins in flat (top) and curved (bottom) POPC bilayers, averaged over the two replicas. The dashed red lines represent the diffusion coefficients from the diagonalization of the diffusion tensor at the corresponding lagtime, while the black curves are the diffusion coefficients along the average major and minor axes of the particle as determined by $\langle\phi_0\rangle$. The green curves are the diffusion coefficients obtained along the *x* and *y* axes of the laboratory frame of reference. Gray dashed line: isotropic diffusion coefficient. Vertical black dashed line: characteristic timescale of diffusion. Horizontal black dashed line: anisotropic diffusion coefficients as averaged from 100 ns to 1.0 μs.

that approximate values produce meaningful results. The primary experimental limitation in applying the Matsuda *et al.* method is the spatial and temporal trajectory resolution. Comparing the two methods is a crucial benchmark that is only possible by using computer simulations where the molecular orientation is known at all times. Fortunately, λ_{SPT} values also indicate a degree of anisotropy that correlates well with λ_{MD}, with $R^2 = 0.8$. The agreement between the two approaches is far from evident regarding the fact the λ_{MD} values were calculated from diffusion coefficients obtained by averaging over relatively large lagtimes, while the λ_{SPT} values are, in principle, more reflective of the $\Delta \to 0$ limiting case. The deviations between the values obtained using these approaches have three major sources. First, the three-step relation inherently only uses information contained in short lagtimes. Second, the procedure completely neglects the orientation of the particle and only uses the information contained in the subsequent translational steps. Finally, the mapping between R_r^2 and λ_{SPT} [Eq. (8)] was derived assuming ideal diffusion, which is typically not a valid assumption.

The *three-step relation* of Matsuda *et al.* does not require the knowledge of the molecular orientation. Modern single-particle imaging techniques are increasingly able to simultaneously reveal both the molecular orientation and translation on timescales and length scales comparable to our MD simulations, thus enabling more sophisticated and illuminating analyses. For the direct measurement of rotational and translational trajectories, one could employ experimental methods such as iSCAT,[80] MINFLUX,[81] or polarized localization microscopy.[48] Super-resolution single-molecule localization microscopy methods (i.e., PALM/STORM)[80,82] are typically limited to localization precision >10 nm, which is greater than the size of most relevant biomolecules. Accordingly, single-molecule localization microscopy is traditionally unable to report the single-molecule orientation for biomolecules labeled with two chromatically distinct fluorophores. Rather than using small-molecule fluorophores, proteins and lipids have been successfully labeled with large fluorescent microspheres such that the localization and orientation of the diffuser could be resolved.[48] If coupled with iSCAT, such a technique has the potential to measure single-molecule localization and orientation on membranes at 1 MHz,[83] but with the complication of having labels orders-of-magnitude larger than the biomolecule. The emerging microscopy method of MINFLUX has demonstrated SPT with single-fluorophore lateral localization precision to 2.4 nm at 40 Hz or 20 nm at 8.5 kHz, depending on the allocation of the photon budget.[81]

Detecting the location and orientation of a single biomolecule with a single fluorophore is feasible by measuring the anisotropic fluorophore emission if the orientation of the fluorophore is chemically coupled to that of the biomolecule. Polarized localization microscopy has been employed to examine the mechanism of motor proteins stepping along actin[84] and nanoscale membrane bending.[85] Optimal conditions may yield a 5 nm two-degree single-fluorophore localization precision with low background, bright fluorophores, and slow imaging.[86] Clever sample preparation provides additional opportunities for connecting experiments to simulations. Imaging live cells has additional challenges of fluorescence background that reduces the localization precision and dynamic variability in the membrane topography. Model bilayers have the potential to isolate key sample parameters with the benefit of controlled membrane composition and shape[87] as well as integrating EM fields and microfluidic flow for dynamic control of sample anisotropy.[88] As demonstrated in our simulations, engineered membrane properties

and protein conformations may regulate the diffusion anisotropy; the methods developed in this manuscript can be applied to analyze the diffusion anisotropy and reveal otherwise irresolvable properties of the underlying membrane or diffusers.

V. CONCLUSIONS

In this work, we provide a framework for extracting parameters describing anisotropy of diffusion from computer simulations. We detect anisotropy using extensive coarse-grained simulations in the regime of microseconds, which is in the reach of current super-resolution SPT measurements.[18,24,76] Notably, our simulations demonstrate that anisotropy can arise either from the molecular shape or from the underlying membrane topology. The strongest anisotropy arises when both are present. Moreover, both integral membrane proteins and peripheral proteins show clear diffusion anisotropy, which is somewhat unexpected.

Simulations provide particle positions and orientations at all timescales and allow to benchmark experimental methods with lesser explicit information. Direct comparison can be achieved by analyzing our trajectories as if they were obtained from SPT measurements, that is, only using molecular positions and the rotational diffusion coefficient of the diffusing particle. By applying the methodology of Matsuda *et al.*[54] to our reduced data, we extracted anisotropy parameters that are in reasonable agreement with those obtained from the more accurate analysis. This is striking when considering their ideal diffusion assumptions but also that probe somewhat different timescales.

The observed anisotropy in motion spanning multi-microsecond timescales may have an impact on diffusion-limited reactions in specific membrane topologies via influencing molecular encounter rates.[89] Moreover, some membrane protein dimers diffuse anisotropically while monomers do not. Using such information and carefully analyzing single-particle tracking data can therefore be used to detect protein oligomerization, which plays a key role in signaling.[1] Similarly, in experiments often limited to probing motion in two dimensions, anisotropy of diffusion could be used as a proxy to study membrane topology.[39,40] We also find that non-symmetric protein–lipid interactions do not really contribute or enhance protein anisotropy as seen in our B_1-AR dimer system. This is somewhat expected, as the dependence of the diffusion coefficient in the Saffman–Delbrück model [Eq. (1)] on many membrane parameters is relatively weak, especially since local changes in membrane viscosity or membrane thickness are relatively small. Finally, our results also contribute to the verification of lateral diffusion models,[90] which are free from symmetry constraints imposed on the particle.

ACKNOWLEDGMENTS

M.J., H.M.-S., P.J., and B.F. acknowledge support from the Czech Science Foundation (EXPRO Grant No. 19-26854X). M.J. acknowledges the CSC–IT Center for Science for computational resources and the Emil Aaltonen Foundation for funding.

APPENDIX A: EQUATIONS OF MOTION OF AN ANISOTROPIC PARTICLE

In the case of an anisotropic particle, the center of diffusion in the laboratory-fixed frame of reference can be given by the following set of equations:

$$\frac{\mathrm{d}}{\mathrm{d}t}\begin{bmatrix} x_1(t) \\ x_2(t) \end{bmatrix} = \begin{bmatrix} \sqrt{2D_\parallel}\cos^2\phi(t) + \sqrt{2D_\perp}\sin^2\phi(t) & \left(\sqrt{2D_\parallel} - \sqrt{2D_\perp}\right)\cos\phi(t)\sin\phi(t) \\ \left(\sqrt{2D_\parallel} - \sqrt{2D_\perp}\right)\cos\phi(t)\sin\phi(t) & \sqrt{2D_\parallel}\sin^2\phi(t) + \sqrt{2D_\perp}\cos^2\phi(t) \end{bmatrix} \cdot \begin{bmatrix} \xi_x(t) \\ \xi_y(t) \end{bmatrix}, \tag{A1}$$

and the rotation of the particle is given by

$$\frac{\mathrm{d}\phi(t)}{\mathrm{d}t} = \sqrt{2D_\mathrm{r}}\xi_r(t), \tag{A2}$$

where $\xi_x(t), \xi_y(t)$, and $\xi_r(t)$ are random forces with $\langle \xi_n(t')\xi_n(t)\rangle = \delta(t'-t)$, $\langle \xi_n(t)\rangle = 0$, $n = x, y, r$. These equations can be integrated in a straightforward manner to obtain the trajectory of the particle.

APPENDIX B: TEMPORAL EVOLUTION OF THE DIFFUSION COEFFICIENTS OF AN ANISOTROPIC PARTICLE

Assuming independent, ideal diffusion along the major and minor axes of the particle, the ensemble average of the time dependent diffusion tensor starting from a fixed ϕ_0 is given by[26]

$$\begin{aligned} D_{xx}(\Delta;\phi_0) &= D + \Delta D\cos 2\phi_0\left(\frac{1-e^{-4D_r\Delta}}{8D_r\Delta}\right), \\ D_{yy}(\Delta;\phi_0) &= D - \Delta D\cos 2\phi_0\left(\frac{1-e^{-4D_r\Delta}}{8D_r\Delta}\right), \\ D_{xy}(\Delta;\phi_0) &= D_{xy}(\Delta) = \Delta D\sin 2\phi_0\left(\frac{1-e^{-4D_r\Delta}}{8D_r\Delta}\right), \end{aligned} \tag{B1}$$

where D is the isotropic diffusion coefficient, $\Delta D = D_\parallel - D_\perp$, D_r is the rotational diffusion coefficient, and Δ is the lagtime. When the reference frame coincides with the principal frame ($\phi_0 = 0$), the diffusion tensor $\mathbf{D}(\Delta;\phi_0 = 0)$ is diagonal at all lagtimes. Otherwise, the diagonal elements converge to D and the off-diagonals to 0 as $\Delta \to \infty$.

APPENDIX C: THE THREE-STEP RELATION OF MATSUDA *et al.*[54]

In their algorithm, Matsuda *et al.* first considered the relative displacements between three consecutive positions $\mathbf{x}_{n-1}$, $\mathbf{x}_n$, and $\mathbf{x}_{n+1}$ along the trajectory, separated by the non-dimensionalized time step $\Delta t'$. The displacements are denoted as $\Delta\mathbf{x}_{n-1} = \mathbf{x}_n - \mathbf{x}_{n-1}$, and $\Delta\mathbf{x}_n = \mathbf{x}_{n+1} - \mathbf{x}_n$, while the non-dimensionalization of the time step is achieved by the relation $\Delta t' = D_r \Delta t$, with Δt being the dimensional time step and D_r being the rotational diffusion coefficient. To allow the reliable detection of anisotropic behavior, $\Delta t' \ll 1$ must hold; otherwise, the anisotropy of the displacements is no longer observable due to rotational averaging. From the relative displacements, a scatter plot is calculated as

$$\begin{bmatrix} \alpha_n \\ \beta_n \end{bmatrix} = \frac{|\Delta\mathbf{x}_n|}{\Delta t'} \begin{bmatrix} \cos\gamma_n \\ \sin\gamma_n \end{bmatrix}, \tag{C1}$$

where γ_n is the angle formed by $\Delta\mathbf{x}_n$ and $\Delta\mathbf{x}_{n-1}$. Finally, the shape of the obtained scatter diagram is characterized by the radius of gyration tensor $\mathbf{R}_g$, which is defined as

$$\mathbf{R}_g^2 = \frac{1}{N} \begin{bmatrix} \sum_{i=1}^{N} (\alpha_i - \langle\alpha\rangle)^2 & \sum_{i=1}^{N} (\alpha_i - \langle\alpha\rangle)(\beta_i - \langle\beta\rangle) \\ \sum_{i=1}^{N} (\alpha_i - \langle\alpha\rangle)(\beta_i - \langle\beta\rangle) & \sum_{i=1}^{N} (\beta_i - \langle\beta\rangle)^2 \end{bmatrix}. \tag{C2}$$

In the limit of $N \to \infty$, the off-diagonal elements vanish, and the diagonals converge to $\langle\alpha^2\rangle$ and $\langle\beta^2\rangle$. The ratio of the diagonal elements, $\langle R_r^2\rangle = \langle\beta^2\rangle / \langle\alpha^2\rangle$, falls in the range $(0, 1]$.

When the particle is completely isotropic, one has $\langle R_r^2\rangle = 1$ and $\lambda = 0$, while $\langle R_r^2\rangle < 1$ indicates a certain degree of anisotropy, therefore corresponding to $\lambda > 0$. Even though the exact relationship between $\langle R_r^2\rangle$ and λ is unknown, the authors make this connection by fitting a simple polynomial equation to results simulated at different values of λ and $\Delta t'$.[54]

DATA AVAILABILITY

The data that support the findings of this study are openly available in Zenodo under reference numbers collected in Table III. The tools used in the analysis can be found at https://github.com/balazsfabian/MD_anisotropy.

TABLE III. DOIs of the performed CG simulations.

System	Geometry	Zenodo doi
F-BAR	Flat	10.5281/zenodo.4114641
	Curved	10.5281/zenodo.4115152
B2AR-monomer	Flat	10.5281/zenodo.4114422
	Curved	10.5281/zenodo.4116245
B2AR-dimer	Flat	10.5281/zenodo.4114065
	Curved	10.5281/zenodo.4115972

REFERENCES

[1] S. Ferré, F. Ciruela, V. Casadó, and L. Pardo, "Oligomerization of G protein-coupled receptors: Still doubted?," in *Progress in Molecular Biology and Translational Science* (Elsevier, 2020), Vol. 169, pp. 297–321.

[2] X. Cong, Y. Liu, W. Liu, X. Liang, and A. Laganowsky, "Allosteric modulation of protein-protein interactions by individual lipid binding events," Nat. Commun. **8**, 2203 (2017).

[3] R. Phillips, T. Ursell, P. Wiggins, and P. Sens, "Emerging roles for lipids in shaping membrane-protein function," Nature **459**, 379–385 (2009).

[4] A. G. Lee, "How lipids affect the activities of integral membrane proteins," Biochim. Biophys. Acta, Biomembr. **1666**, 62–87 (2004).

[5] V. Corradi, E. Mendez-Villuendas, H. I. Ingólfsson, R.-X. Gu, I. Siuda, M. N. Melo, A. Moussatova, L. J. DeGagné, B. I. Sejdiu, G. Singh *et al.*, "Lipid–protein interactions are unique fingerprints for membrane proteins," ACS Cent. Sci. **4**, 709–717 (2018).

[6] M. F. Brown, "Soft matter in lipid–protein interactions," Annu. Rev. Biophys. **46**, 379–410 (2017).

[7] S. Sarkar, "Concentration dependence of diffusion-limited reaction rates and its consequences," Phys. Rev. X **10**, 041032 (2020).

[8] P. D. Calvert, V. I. Govardovskii, N. Krasnoperova, R. E. Anderson, J. Lem, and C. L. Makino, "Membrane protein diffusion sets the speed of rod phototransduction," Nature **411**, 90–94 (2001).

[9] A. J. B. Kreutzberger, M. Ji, J. Aaron, L. Mihaljević, and S. Urban, "Rhomboid distorts lipids to break the viscosity-imposed speed limit of membrane diffusion," Science **363**, eaao0076 (2019).

[10] L. Wawrezinieck, H. Rigneault, D. Marguet, and P.-F. Lenne, "Fluorescence correlation spectroscopy diffusion laws to probe the submicron cell membrane organization," Biophys. J. **89**, 4029–4042 (2005).

[11] S. Sadegh, J. L. Higgins, P. C. Mannion, M. M. Tamkun, and D. Krapf, "Plasma membrane is compartmentalized by a self-similar cortical actin meshwork," Phys. Rev. X **7**, 011031 (2017).

[12] A. Weron, K. Burnecki, E. J. Akin, L. Solé, M. Balcerek, M. M. Tamkun, and D. Krapf, "Ergodicity breaking on the neuronal surface emerges from random switching between diffusive states," Sci. Rep. **7**, 5404 (2017).

[13] K. M. Spillane, J. Ortega-Arroyo, G. de Wit, C. Eggeling, H. Ewers, M. I. Wallace, and P. Kukura, "High-speed single-particle tracking of GM1 in model membranes reveals anomalous diffusion due to interleaflet coupling and molecular pinning," Nano Lett. **14**, 5390–5397 (2014).

[14] P. M. Winkler, R. Regmi, V. Flauraud, J. Brugger, H. Rigneault, J. Wenger, and M. F. García-Parajo, "Transient nanoscopic phase separation in biological lipid membranes resolved by planar plasmonic antennas," ACS Nano **11**, 7241–7250 (2017).

[15] G. Vicidomini, H. Ta, A. Honigmann, V. Mueller, M. P. Clausen, D. Waithe, S. Galiani, E. Sezgin, A. Diaspro, S. W. Hell, and C. Eggeling, "STED-FLCS: An advanced tool to reveal spatiotemporal heterogeneity of molecular membrane dynamics," Nano Lett. **15**, 5912–5918 (2015).

[16] F. Schneider, D. Waithe, B. C. Lagerholm, D. Shrestha, E. Sezgin, C. Eggeling, and M. Fritzsche, "Statistical analysis of scanning fluorescence correlation spectroscopy data differentiates free from hindered diffusion," ACS Nano **12**, 8540–8546 (2018).

[17] C. Eggeling, C. Ringemann, R. Medda, G. Schwarzmann, K. Sandhoff, S. Polyakova, V. N. Belov, B. Hein, C. Von Middendorff, A. Schönle, and S. W. Hell, "Direct observation of the nanoscale dynamics of membrane lipids in a living cell," Nature **457**, 1159–1162 (2009).

[18] L. Schermelleh, A. Ferrand, T. Huser, C. Eggeling, M. Sauer, O. Biehlmaier, and G. P. C. Drummen, "Super-resolution microscopy demystified," Nat. Cell Biol. **21**, 72–84 (2019).

[19] S. J. Sahl, M. Leutenegger, M. Hilbert, S. W. Hell, and C. Eggeling, "Fast molecular tracking maps nanoscale dynamics of plasma membrane lipids," Proc. Natl. Acad. Sci. U. S. A. **107**, 6829–6834 (2010).

[20] H.-M. Wu, Y.-H. Lin, T.-C. Yen, and C.-L. Hsieh, "Nanoscopic substructures of raft-mimetic liquid-ordered membrane domains revealed by high-speed single-particle tracking," Sci. Rep. **6**, 20542 (2016).

[21] J. Ortega Arroyo, J. Andrecka, K. M. Spillane, N. Billington, Y. Takagi, J. R. Sellers, and P. Kukura, "Label-free, all-optical detection, imaging, and tracking of a single protein," Nano Lett. **14**, 2065–2070 (2014).
[22] E. Mobarak, M. Javanainen, W. Kulig, A. Honigmann, E. Sezgin, N. Aho, C. Eggeling, T. Rog, and I. Vattulainen, "How to minimize dye-induced perturbations while studying biomembrane structure and dynamics: PEG linkers as a rational alternative," Biochim. Biophys. Acta, Biomembr. **1860**, 2436–2445 (2018).
[23] A. A. Gurtovenko, M. Javanainen, F. Lolicato, and I. Vattulainen, "The devil is in the details: What do we really track in single-particle tracking experiments of diffusion in biological membranes?," J. Phys. Chem. Lett. **10**, 1005–1011 (2019).
[24] C. Manzo and M. F. Garcia-Parajo, "A review of progress in single particle tracking: From methods to biophysical insights," Rep. Prog. Phys. **78**, 124601 (2015).
[25] I. Casuso, J. Khao, M. Chami, P. Paul-Gilloteaux, M. Husain, J.-P. Duneau, H. Stahlberg, J. N. Sturgis, and S. Scheuring, "Characterization of the motion of membrane proteins using high-speed atomic force microscopy," Nat. Nanotechnol. **7**, 525–529 (2012).
[26] Y. Han, A. M. Alsayed, M. Nobili, J. Zhang, T. C. Lubensky, and A. G. Yodh, "Brownian motion of an ellipsoid," Science **314**, 626–630 (2006).
[27] F. Perrin, E. Stahel, H. Ketelaar, J. Dufay, J. Gauzit, S. Gawronski, S. Gawronski, M. Meunier, J. Andriot, A. Piekara *et al.*, "Brownian motion of an ellipsoid. I. Dielectric dispersion for ellipsoidal molecules. Mouvement Brownien d'un ellipsoide. I. Dispersion diélectrique pour des molécules ellipsoidales," J. Phys. Radium **5**, 497 (1934).
[28] J. F. Ellena, P. Lackowicz, H. Mongomery, and D. S. Cafiso, "Membrane thickness varies around the circumference of the transmembrane protein BtuB," Biophys. J. **100**, 1280–1287 (2011).
[29] M. Długosz and J. M. Antosiewicz, "Transient effects of excluded volume interactions on the translational diffusion of hydrodynamically anisotropic molecules," J. Chem. Theory Comput. **10**, 2583–2590 (2014).
[30] F. Perrin, "Mouvement Brownien d'un ellipsoide. II. Rotation libre et dépolarisation des fluorescences. Translation et diffusion de molécules ellipsoidales," J. Phys. Radium **7**, 1–11 (1936).
[31] A. Chakrabarty, A. Konya, F. Wang, J. V. Selinger, K. Sun, and Q.-H. Wei, "Brownian motion of arbitrarily shaped particles in two dimensions," Langmuir **30**, 13844–13853 (2014).
[32] M. S. Strano and H. Jin, "Where is it heading? Single-particle tracking of single-walled carbon nanotubes," ACS Nano **2**, 1749–1752 (2008).
[33] M. Schwartz, D. Duan, and R. J. Berry, "Molecular dynamics study of anisotropic translational and rotational diffusion in liquid benzene," J. Phys. Chem. A **109**, 8637–8641 (2005).
[34] R. Vasanthi, S. Ravichandran, and B. Bagchi, "Needlelike motion of prolate ellipsoids in the sea of spheres," J. Chem. Phys. **114**, 7989–7992 (2001).
[35] R. Vasanthi, S. Ravichandran, and B. Bagchi, "Anisotropic diffusion of tagged spheres near the isotropic-nematic phase transition," J. Chem. Phys. **115**, 10022–10028 (2001).
[36] Z.-T. Zhang, X. Zhao, and B.-Y. Cao, "Diffusion tensors of arbitrary-shaped nanoparticles in fluid by molecular dynamics simulation," Sci. Rep. **9**, 18943 (2019).
[37] A. N. Rissanou, P. Bačová, and V. Harmandaris, "Investigation of the properties of nanographene in polymer nanocomposites through molecular simulations: Dynamics and anisotropic Brownian motion," Phys. Chem. Chem. Phys. **21**, 23843–23854 (2019).
[38] Y. Han, A. Alsayed, M. Nobili, and A. G. Yodh, "Quasi-two-dimensional diffusion of single ellipsoids: Aspect ratio and confinement effects," Phys. Rev. E **80**, 011403 (2009).
[39] A. Gesper, S. Wennmalm, P. Hagemann, S.-G. Eriksson, P. Happel, and I. Parmryd, "Variations in plasma membrane topography can explain heterogenous diffusion coefficients obtained by fluorescence correlation spectroscopy," Front. Cell Dev. Biol. **8**, 767 (2020).
[40] J. Adler, I.-M. Sintorn, R. Strand, and I. Parmryd, "Conventional analysis of movement on non-flat surfaces like the plasma membrane makes Brownian motion appear anomalous," Commun. Biol. **2**, 12 (2019).
[41] M. Javanainen, H. Martinez-Seara, R. Metzler, and I. Vattulainen, "Diffusion of integral membrane proteins in protein-rich membranes," J. Phys. Chem. Lett. **8**, 4308–4313 (2017).
[42] P. G. Saffman and M. Delbrück, "Brownian motion in biological membranes," Proc. Natl. Acad. Sci. U. S. A. **72**, 3111–3113 (1975).
[43] F. Jähnig, "The shape of a membrane protein derived from rotational diffusion," Eur. Biophys. J. **14**, 63–64 (1986).
[44] J. H. Werner, G. A. Montaño, A. L. Garcia, N. A. Zurek, E. A. Akhadov, G. P. Lopez, and A. P. Shreve, "Formation and dynamics of supported phospholipid membranes on a periodic nanotextured substrate," Langmuir **25**, 2986–2993 (2009).
[45] T. Yoshigaki, "Theoretically predicted effects of Gaussian curvature on lateral diffusion of membrane molecules," Phys. Rev. E **75**, 041901 (2007).
[46] H. T. McMahon and E. Boucrot, "Membrane curvature at a glance," J. Cell Sci. **128**, 1065–1070 (2015).
[47] M. J. Saxton, "Single-particle tracking: Connecting the dots," Nat. Methods **5**, 671–672 (2008).
[48] T. T. Hormel, S. Q. Kurihara, M. K. Brennan, M. C. Wozniak, and R. Parthasarathy, "Measuring lipid membrane viscosity using rotational and translational probe diffusion," Phys. Rev. Lett. **112**, 188101 (2014).
[49] J. Myšková, O. Rybakova, J. Brynda, P. Khoroshyy, A. Bondar, and J. Lazar, "Directionality of light absorption and emission in representative fluorescent proteins," Proc. Natl. Acad. Sci.U. S. A. **117**, 32395–32401 (2020).
[50] S. A. Rosenberg, M. E. Quinlan, J. N. Forkey, and Y. E. Goldman, "Rotational motions of macro-molecules by single-molecule fluorescence microscopy," Acc. Chem. Res. **38**, 583–593 (2005).
[51] J.-H. Jeon, H. M.-S. Monne, M. Javanainen, and R. Metzler, "Anomalous diffusion of phospholipids and cholesterols in a lipid bilayer and its origins," Phys. Rev. Lett. **109**, 188103 (2012).
[52] M. Javanainen, H. Hammaren, L. Monticelli, J.-H. Jeon, M. S. Miettinen, H. Martinez-Seara, R. Metzler, and I. Vattulainen, "Anomalous and normal diffusion of proteins and lipids in crowded lipid membranes," Faraday Discuss. **161**, 397–417 (2013).
[53] A. L. Duncan, T. Reddy, H. Koldsø, J. Hélie, P. W. Fowler, M. Chavent, and M. S. Sansom, "Protein crowding and lipid complexity influence the nanoscale dynamic organization of ion channels in cell membranes," Sci. Rep. **7**, 16647 (2017).
[54] Y. Matsuda, I. Hanasaki, R. Iwao, H. Yamaguchi, and T. Niimi, "Faster convergence of diffusion anisotropy detection by three-step relation of single-particle trajectory," Anal. Chem. **88**, 4502–4507 (2016).
[55] S. J. Marrink, H. J. Risselada, S. Yefimov, D. P. Tieleman, and A. H. De Vries, "The Martini force field: Coarse grained model for biomolecular simulations," J. Phys. Chem. B **111**, 7812–7824 (2007).
[56] L. Monticelli, S. K. Kandasamy, X. Periole, R. G. Larson, D. P. Tieleman, and S.-J. Marrink, "The Martini coarse-grained force field: Extension to proteins," J. Chem. Theory Comput. **4**, 819–834 (2008).
[57] B. J. Peter, H. M. Kent, I. G. Mills, Y. Vallis, P. J. G. Butler, P. R. Evans, and H. T. McMahon, "Bar domains as sensors of membrane curvature: The amphiphysin bar structure," Science **303**, 495–499 (2004).
[58] J. Huang, S. Chen, J. J. Zhang, and X.-Y. Huang, "Crystal structure of oligomeric β1-adrenergic G protein–coupled receptors in ligand-free basal state," Nat. Struct. Mol. Biol. **20**, 419 (2013).
[59] R. Metzler, J.-H. Jeon, A. G. Cherstvy, and E. Barkai, "Anomalous diffusion models and their properties: Non-stationarity, non-ergodicity, and ageing at the centenary of single particle tracking," Phys. Chem. Chem. Phys. **16**, 24128–24164 (2014).
[60] C. Ribrault, A. Triller, and K. Sekimoto, "Diffusion trajectory of an asymmetric object: Information overlooked by the mean square displacement," Phys. Rev. E **75**, 021112 (2007).
[61] I. Hanasaki and Y. Isono, "Detection of diffusion anisotropy due to particle asymmetry from single-particle tracking of Brownian motion by the large-deviation principle," Phys. Rev. E **85**, 051134 (2012).

[62]B. Bhaduri, A. Neild, and T. W. Ng, "Directional Brownian diffusion dynamics with variable magnitudes," Appl. Phys. Lett. **92**, 084105 (2008).
[63]M. Linke, J. Köfinger, and G. Hummer, "Fully anisotropic rotational diffusion tensor from molecular dynamics simulations," J. Phys. Chem. B **122**, 5630–5639 (2018).
[64]M. J. Abraham, T. Murtola, R. Schulz, S. Páll, J. C. Smith, B. Hess, and E. Lindahl, "GROMACS: High performance molecular simulations through multi-level parallelism from laptops to supercomputers," SoftwareX **1-2**, 19–25 (2015).
[65]B. Kohnke, C. Kutzner, and H. Grubmüller, "A GPU-accelerated fast multipole method for GROMACS: Performance and accuracy," J. Chem. Theory Comput. **16**, 6938–6949 (2020).
[66]J.-H. Jeon, M. Javanainen, H. Martinez-Seara, R. Metzler, and I. Vattulainen, "Protein crowding in lipid bilayers gives rise to non-Gaussian anomalous lateral diffusion of phospholipids and proteins," Phys. Rev. X **6**, 021006 (2016).
[67]L. A. Rowley, D. Nicholson, and N. G. Parsonage, "Monte Carlo grand canonical ensemble calculation in a gas-liquid transition region for 12-6 argon," J. Comput. Phys. **17**, 401–414 (1975).
[68]G. Bussi, D. Donadio, and M. Parrinello, "Canonical sampling through velocity rescaling," J. Chem. Phys. **126**, 014101 (2007).
[69]W. M. Henne, H. M. Kent, M. G. J. Ford, B. G. Hegde, O. Daumke, P. J. G. Butler, R. Mittal, R. Langen, P. R. Evans, and H. T. McMahon, "Structure and analysis of FCHo2 F-bar domain: A dimerizing and membrane recruitment module that effects membrane curvature," Structure **15**, 839–852 (2007).
[70]M. Simunovic, C. Prévost, A. Callan-Jones, and P. Bassereau, "Physical basis of some membrane shaping mechanisms," Philos. Trans. R. Soc., A **374**, 20160034 (2016).
[71]K. J. Boyd and E. R. May, "BUMPy: A model-independent tool for constructing lipid bilayers of varying curvature and composition," J. Chem. Theory Comput. **14**, 6642–6652 (2018).
[72]D. H. De Jong, S. Baoukina, H. I. Ingólfsson, and S. J. Marrink, "Martini straight: Boosting performance using a shorter cutoff and GPUs," Comput. Phys. Commun. **199**, 1–7 (2016).
[73]R. M. Venable, H. I. Ingólfsson, M. G. Lerner, B. S. Perrin, Jr., B. A. Camley, S. J. Marrink, F. L. H. Brown, and R. W. Pastor, "Lipid and peptide diffusion in bilayers: The Saffman–Delbrück model and periodic boundary conditions," J. Phys. Chem. B **121**, 3443–3457 (2017).
[74]M. Javanainen, O. H. S. Ollila, and H. Martinez-Seara, "Rotational diffusion of membrane proteins in crowded membranes," J. Phys. Chem. B **124**, 2994–3001 (2020).
[75]M. Vögele, J. Köfinger, and G. Hummer, "Hydrodynamics of diffusion in lipid membrane simulations," Phys. Rev. Lett. **120**, 268104 (2018).
[76]H. Shen, L. J. Tauzin, R. Baiyasi, W. Wang, N. Moringo, B. Shuang, and C. F. Landes, "Single particle tracking: From theory to biophysical applications," Chem. Rev. **117**, 7331–7376 (2017).
[77]R. W. Taylor, R. G. Mahmoodabadi, V. Rauschenberger, A. Giessl, A. Schambony, and V. Sandoghdar, "Interferometric scattering microscopy reveals microsecond nanoscopic protein motion on a live cell membrane," Nat. Photonics **13**, 480–487 (2019).
[78]R. Grima and S. N. Yaliraki, "Brownian motion of an asymmetrical particle in a potential field," J. Chem. Phys. **127**, 084511 (2007).
[79]A. Naji and F. L. Brown, "Diffusion on ruffled membrane surfaces," J. Chem. Phys. **126**, 235103 (2007).
[80]E. Betzig, G. H. Patterson, R. Sougrat, O. W. Lindwasser, S. Olenych, J. S. Bonifacino, M. W. Davidson, J. Lippincott-Schwartz, and H. F. Hess, "Imaging intracellular fluorescent proteins at nanometer resolution," Science **313**, 1642–1645 (2006).
[81]R. Schmidt, T. Weihs, C. A. Wurm, I. Jansen, J. Rehman, S. J. Sahl, and S. W. Hell, "MINFLUX nanometer-scale 3D imaging and microsecond-range tracking on a common fluorescence microscope," Nat. Commun. **12**, 1478 (2021).
[82]S. Van de Linde, A. Löschberger, T. Klein, M. Heidbreder, S. Wolter, M. Heilemann, and M. Sauer, "Direct stochastic optical reconstruction microscopy with standard fluorescent probes," Nat. Protoc. **6**, 991 (2011).
[83]G. Young and P. Kukura, "Interferometric scattering microscopy," Annu. Rev. Phys. Chem. **70**, 301–322 (2019).
[84]J. N. Forkey, M. E. Quinlan, and Y. E. Goldman, "Measurement of single macromolecule orientation by total internal reflection fluorescence polarization microscopy," Biophys. J. **89**, 1261–1271 (2005).
[85]A. M. Kabbani and C. V. Kelly, "The detection of nanoscale membrane bending with polarized localization microscopy," Biophys. J. **113**, 1782–1794 (2017).
[86]F. Aguet, S. Geissbühler, I. Märki, T. Lasser, and M. Unser, "Super-resolution orientation estimation and localization of fluorescent dipoles using 3-D steerable filters," Opt. Express **17**, 6829–6848 (2009).
[87]X. Woodward, E. E. Stimpson, and C. V. Kelly, "Single-lipid tracking on nanoscale membrane buds: The effects of curvature on lipid diffusion and sorting," Biochim. Biophys. Acta, Biomembr. **1860**, 2064–2075 (2018).
[88]C. V. Kelly and H. G. Craighead, "Nanofabrication for the analysis and manipulation of membranes," Ann. Biomed. Eng. **40**, 1356–1366 (2012).
[89]M. Długosz and J. M. Antosiewicz, "Anisotropic diffusion effects on the Barnase–Barstar encounter kinetics," J. Chem. Theory Comput. **9**, 1667–1677 (2013).
[90]B. A. Camley and F. L. H. Brown, "Motion of objects embedded in lipid bilayer membranes: Advection and effective viscosity," J. Chem. Phys. **151**, 124104 (2019).